BBA - Molecular Basis of Disease 1865 (2019) 165552

Contents lists available at ScienceDirect

BBA - Molecular Basis of Disease

journal homepage: www.elsevier.com/locate/bbadis

mTORC1 inhibition attenuates necroptosis through RIP1 inhibition-mediated TFEB activation

Koki Abe[a,1], Toshiyuki Yano[a,1], Masaya Tanno[a], Takayuki Miki[a], Atsushi Kuno[a,b], Tatsuya Sato[a,c], Hidemichi Kouzu[a], Kei Nakata[a], Wataru Ohwada[a], Yukishige Kimura[a], Hirohito Sugawara[a], Satoru Shibata[a], Yusuke Igaki[a], Shoya Ino[a], Tetsuji Miura[a,*]

[a] Department of Cardiovascular, Renal and Metabolic Medicine, Sapporo Medical University School of Medicine, Sapporo, Japan
[b] Department of Pharmacology, Sapporo Medical University School of Medicine, Sapporo, Japan
[c] Department of Cell Physiology and Signal Transduction, Sapporo Medical University School of Medicine, Sapporo, Japan

ARTICLE INFO

Keywords:
Necroptosis
Autophagy
RIP1
TNF-α
Rapamycin
mTOR

ABSTRACT

Accumulating evidence indicates that necroptosis contributes to cardiovascular diseases. We recently reported suppression of autophagy by necroptotic signals in cardiomyocytes and protective action of rapamycin. Here we examined the mechanism by which mTORC1 inhibition protects cardiomyocytes from necroptosis. Necroptosis of H9c2 cells was induced by treatment with tumor necrotic factor-α (TNF) and z-VAD-fmk (zVAD), and the extent of necroptosis was determined as the level of LDH release (as % of total). TNF/zVAD increased RIP1-RIP3 interaction and LDH release from 3.4 ± 1.3% to 46.1 ± 2.3%. The effects of TNF/zVAD were suppressed by an mTORC1 inhibitor, rapamycin, and an mTORC1/2 inhibitor, Ku-0063794, but not by a p70s6K inhibitor, PF-4708671. Protection by rapamycin was not abolished by inhibitors of TAK1, IKKα/β, and cIAP, endogenous necroptosis suppressors upstream of RIP1. Rapamycin and Ku-0063794 suppressed TNF/zVAD-induced RIP1-Ser166 phosphorylation and increased phosphorylation of RIP1-Ser320, an inhibitory phosphorylation site, though such an effect on RIP1-Ser320 was not observed for PF-4708671. Protective effects of rapamycin on TNF/zVAD-induced RIP1-RIP3 binding and necroptosis were undetected in cells transfected with RIP1-S320A. In TNF/zVAD-treated cells, rapamycin and a RIP1 inhibitor, necrostatin-1, increased nuclear localization of transcriptional factor EB (TFEB) and promoted autolysosome formation from autophagosomes in a TFEB-dependent manner. Knockdown of TFEB expression attenuated rapamycin-induced protection from necroptosis in TNF/zVAD-treated cells. The results suggest that mTORC1 inhibition promotes autophagy and protects cardiomyocytes from necroptosis by a TFEB-dependent mechanism and that inhibition of RIP1 by increased phosphorylation at Ser320 is crucial in the cardiomyocyte protection afforded by mTORC1 inhibition.

1. Introduction

Necroptosis, a form of programmed necrosis, has been shown to contribute to the pathogenesis of inflammatory diseases including viral infection, inflammatory bowel disease [1–4] and cardiac diseases [5–8]. In addition, recent studies have shown that caspase-8 and TAK1 levels were downregulated in end-stage heart failure [9,10], which increases the propensity for necroptosis [10–12]. The most widely investigated initiator of the necroptotic pathway is tumor necrosis factor-α (TNF). Activation of the TNF receptor induces rapid recruitment of TNF receptor I-associated death domain protein (TRADD), receptor-interacting protein 1 (RIP1), TNF receptor-associated factor 2 (TRAF2), and cellular inhibitor apoptosis proteins (cIAPs), subsequently leading to the formation of a cytosolic death-inducing signaling complex (complex IIa) including Fas-associated death domain (FADD) and caspase-8. Formation of complex IIa is followed by self-cleavage of caspase-8, leading to caspase-3-mediated apoptosis [1–4]. When activation of caspase-8 is perturbed, necroptosis is induced by formation of canonical necrosomes consisting of RIP1 and RIP3, which leads to plasma membrane disruption by translocation of oligomerized mixed lineage kinase domain-like (MLKL) molecules [1–4,13–17]. In contrast to necroptosis of inflammatory cells and fibroblasts, cardiomyocyte necroptosis has not been characterized fully.

* Corresponding author at: Department of Cardiovascular, Renal, and Metabolic Medicine, Sapporo Medical University School of Medicine, South-1, West-16, Chuo-ku, Sapporo 060-8543, Japan.
E-mail address: miura@sapmed.ac.jp (T. Miura).
[1] The two authors contributed equally to this work.

https://doi.org/10.1016/j.bbadis.2019.165552
Received 14 April 2019; Received in revised form 22 August 2019; Accepted 4 September 2019
Available online 06 September 2019

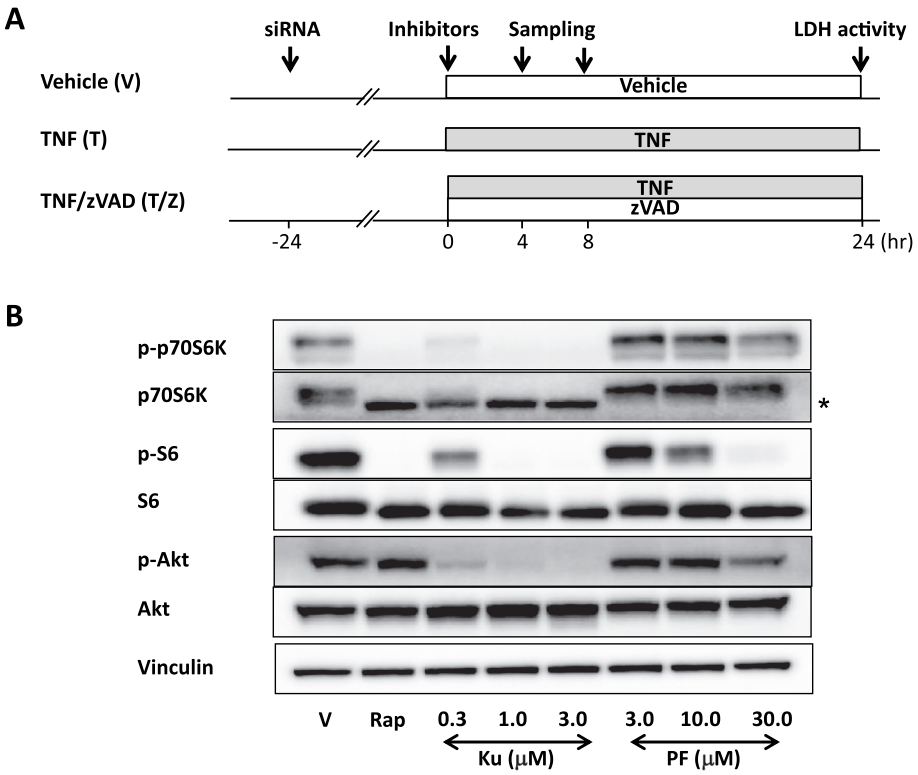

Fig. 1. Effects of mTOR inhibitors and a p70s6K inhibitor on TNF/zVAD-induced cell death.
(A) Experimental protocols. H9c2 cells were treated with a vehicle (V), TNF-α (T; 50 ng/ml), or TNF-α and zVAD (T/Z, zVAD; 20 μM). Samples for analyses were collected at 4, 8 and 24 h after the addition of each agent. (B) Effects of mTOR inhibitors and a p70s6K inhibitor on Akt/mTOR/p70s6K signaling. Representative Western blots for phosphorylated and total p70s6K, S6 and Akt are shown. p-p70s6K = phospho-Thr389-p70s6K, p-S6 = phospho-Ser235/236-ribosomal protein S6, pAkt = phospho-Ser473-Akt. Vinculin was used as a loading control. V = vehicle, Rap = rapamycin, Ku = Ku-0063794, PF = PF-4708671. Asterisk (*) indicates band shifts of dephosphorylated p70s6K. (C) Effects of mTOR inhibitors and a p70s6K inhibitor on T/Z-induced cell death. LDH release into the culture medium as a percentage of the total cellular LDH activity was used as an index of cell death. N = 6 in each group. *$p < 0.05$ vs. V. $^{\dagger}p < 0.05$ vs. T/Z + V.

Autophagy is an endogenous protective machinery against pathological stresses including myocardial infarction [18–21]. In addition, a bidirectional effect of autophagy on programmed cell death including apoptosis and necroptosis has been reported [22–25]. Recently, we examined the crosstalk between autophagy and necroptosis in H9c2 cardiomyoblasts [26]. Stimulation of the TNF receptor together with suppression of caspase activity by z-VAD-fmk (zVAD), a pan-caspase inhibitor, induced RIP1/RIP3-dependent necroptosis. Activation of the necroptotic pathway by TNF/zVAD did not affect phosphorylation of protein kinases that inhibit autophagy (Akt and p70s6K, a kinase downstream of the mechanistic target of rapamycin [mTORC1]) and/or activate autophagy (AMPK, ULK1 and PKA) [26]. However, TNF/zVAD disturbed fusion of autophagosomes and lysosomes, suppressing autophagic flux [26]. Interestingly, treatment with rapamycin restored TNF/zVAD-induced disturbance of autophagic flux, which was associated with mitigation of necroptosis. However, molecular mechanisms by which rapamycin improved autophagic flux and prevented necroptosis in TNF/zVAD-treated cells remained unclear. To address the issues, the present study was designed to systematically examine the effect of mTORC1 inhibition on signaling pathways regulating necroptosis and autophagy. We particularly focused on regulatory mechanisms of RIP1 by mTORC1 and a role of transcriptional factor EB (TFEB) in impairment of autophagy by activation of necroptosis signals.

2. Methods

2.1. Chemical compounds

TNF-α, bafilomycin A1, Ku-0063794, PF-4708671, 5z-7-oxozeaenol, TPCA-1, and nutlin-3 were purchased from Sigma Aldrich (St. Louis, MO). Z-Val-Ala-DL-Asp-fluoromethylketone (zVAD) from Promega (Madison, WI), necrostatin-1 from Calbiochem (San Diego, CA), rapamycin from Cell Signaling Technology (Beverly, MA), and BV6 from ApexBio Technology (Houston, TX) were used. Vectors of green fluorescent protein-red fluorescent protein-LC3 tandem protein (RFP-GFP-LC3) were obtained from Addgene (Osaka, Japan).

2.2. Cell culture and transfection

H9c2 cells, rat cardiomyoblast cells, were obtained from ATCC (American Type Culture Collection). The cells were cultured in Dulbecco's Modified Eagle's Medium (4.5 g/L glucose) supplemented with 10% fetal bovine serum and antibiotics. Knockdown of RIP3, MLKL, ULK1, and p53 was performed by transfection of siRNA against rat RIP3 (L-096899, Dharmacon, Lafayette, CO), rat MLKL (L-11341-00-0005, Dharmacon), rat ULK1 (L-081408-02-0005, Dharmacon), and rat p53 (L-

040642-00-0005, Dharmacon) using Lipofectamine™ RNAiMAX (Thermo Fisher Scientific, Waltham, MA) according to the manufacturer's protocol. The HA-RIP1-WT plasmid (RIP1-WT) (pCMV-HA-C Vector; Takara Bio Inc. 635690, Shiga, Japan), HA-RIP1-Ser414A (RIP1-S414A), HA-RIP1-Ser320A (RIP1-S320A), HA-RIP1-Ser320D (RIP1-S320D), and HA-RIP1-Ser335A (RIP1-S335A) were transfected into H9c2 cells using FuGENE HD (Promega, Madison, WI). A QuikChange Lightening mutagenesis kit (Stratagene) was used for site-directed mutagenesis of RIP1, and the primer sets for mutated RIP1 were as follows: RIP1-S414A (forward, 5′-gaagcgaagggtcgcccatgacccctttg-3′; reverse, 5′-caaaggggtcatgggcgaccctcgcttc-3′), RIP1-S320A (forward, 5′-cccagttttgaagagaatgtttgctctgcagcatgactg-3′; reverse, 5′-cagtcatgctgcagagcaaacattctcttcaaaactggg-3′), RIP1-S320D (forward, 5′-gaagagaatgtttgacctgcagcatgact-3′; reverse, 5′-agtcatgctgcaggtcaaacattctcttc-3′), RIP1-S335A (forward, 5′-cctccaagcaggtcaaatgcagaacaacccggt-3′; reverse, 5′-accgggttgttctgcatttgacctgcttggagg-3′). Experiments were completed 24–48 h after transfection.

Neonatal rat ventricular myocytes (NRVM) were isolated from the whole heart of 1–3 days old rats. In brief, the hearts were minced, digested with trypsin overnight at 4 °C. The day after, tissue was dissociated by stepwise collagenase treatment for a few minutes at 37 °C. Cells were pre-plated twice for 60 min to eliminate fibroblasts and enrich the culture for cardiac myocytes. The non-adherent myocytes were then plated at a density of 1200 cells/mm^2 in plating medium consisting of 199 medium supplemented with HEPES, MEM non-essential amino acids, glucose, glutamine, 10% FBS, vitamin B12, penicillin, streptomycin, on fibronectin coated plates. The next day cells were washed and fresh medium with 2% FBS was added. The cells were maintained at 37 °C in the presence of 5% CO_2 in a humidified incubator.

2.3. Experimental protocols

H9c2 cells were assigned to 4-h, 8-h or 24-h treatment with the combination of 2.89 μM (50 ng/ml) TNF-α and 20 μM zVAD (TNF/zVAD), TNF-α alone, or a vehicle (Fig. 1A). The doses of TNF-α and zVAD were selected as doses that induce 50% cell death after 24-h treatment based on the results of our previous study [26]. Inhibitors of RIP1 (50 μM of necrostatin-1), mTORC1 (10 nM of rapamycin), both mTORC1 and mTORC2 (1 μM of KU-0063794), p70s6K (30 μM of PF-4708671), TAK1 (10–100 nM of 5z-7-Oxozeaenol), IKKα/β (100–250 nM of TPCA-1), cIAP (0.3–1 nM of BV6), p53 (10 μM of pifithrin-α), MDM2 (10 μM of nutlin-3) and autophagic flux (100 nM of bafilomycin A1) were each added to the culture medium at the same time as cells received TNF/zVAD or its control agents. Transfection with siRNA of RIP3, MLKL, ULK1, and p53 was performed 24–48 h before the addition of pharmacological agents.

2.4. Western blotting and immunoprecipitation

To obtain whole cell lysates, samples were homogenized in a lysis buffer (CelLytic M, Sigma Aldrich, St. Louis, MO), a protease inhibitor cocktail (Complete mini, Roche Molecular Biochemicals, Mannheim, Germany), and a phosphatase inhibitor cocktail (PhosSTOP, Roche Molecular Biochemicals). The homogenate was centrifuged at 13,000*g* for 15 min to obtain the supernatant. Fractionation of nuclei and cytosol were performed by the method reported by Yonekawa et al. [27]. Protein concentration was determined using the Bradford assay. Equal amounts of proteins were electrophoresed on 7.5% or 12.5% polyacrylamide gels and then blotted onto PVDF membranes (Millipore, Bedford, MA). After blocking had been performed with a TBS-T buffer containing 5% nonfat dry milk or 5% BSA, the blots were incubated with antibodies that recognize the following: phospho-p70s6K (Thr389) and p70s6K, phospho-Akt (Ser473) and total Akt, phospho-ribosomal protein S6 (Ser237/238) and total ribosomal protein S6, phospho-RIP1 (Ser166), phospho-RIP1 (Ser321), and RIP1, RIP3, TRAF2, cIAP, TAK1, caspase-8, phospho-AMPK (Thr172) and AMPK, phospho-ACC (Ser79) and ACC, phospho-ULK1 (Ser317) and phospho-ULK1 (Ser757), phospho-p38 (Thr180/Tyr182) and p38, phospho-IKKα/β (Ser176/180) and IKKβ, phospho-IκBα (Ser32) and IκBα, phospho-p65 (Ser536) and p65, p62, LC3, PUMA (Cell Signaling Technology, Beverly, MA); ULK1 and FADD (Abcam, Cambridge, UK); MLKL (Merck Millipore, Damstadt, Germany); TFEB (Proteintech, Chicago, IL); p53, cylindromatosis 1, A20 (Santa Cruz Biotechnology, Dallas, TX); RIP1 (BD Biosciences, San Jose, CA); and vinculin (Sigma Aldrich, St Louis, MO). To examine phosphorylation at the RXX(S*/T*) motif of rat RIP1, anti-phospho-RXRXX(S*/T*) antibody (cat#10001, Cell Signaling) that cross reacts with phospho-RXX(S*/T*) motifs was used since anti-phospho-RXX(S*/T*) was unavailable at the time we commenced the present project. Immunoblotted proteins were visualized by using an Immobilon Western detection kit (Millipore, Billerica, MA). Protein interactions were analyzed by immunoprecipitation experiments. Precleared cell lysates (500 μg) were incubated with 2 μg of anti-RIP1 antibody, 3 μl of anti-p62 antibody, or 5 μl of anti-RIP3 antibody in ice-cold lysis buffer at 4 °C overnight with rotation. Antibody-protein complexes were collected with magnet beads and washed with ice-cold lysis buffer. Immunoprecipitates were subjected to Western blotting as described above. Proteins detected by Western blotting were quantified by measuring intensities of individual bands by using Image J software (National Institutes of Health).

2.5. LDH activity assay

The extent of cell death was determined by quantifying lactate dehydrogenase (LDH) released into the culture medium as previously reported [26]. LDH activity in the culture medium and LDH activity after freeze-thawing of the cells (total cellular LDH activity) were measured by using a CytoTox 96 Non-Radioactive Cytotoxicity assay kit (Promega, Madison, WI) according to the manufacturer's protocol. LDH release from cells was expressed as a percentage of the total cellular LDH activity.

2.6. Fluorescence microscopy experiments

Assessment of autophagic flux: An assay using the RFP-GFP-LC3 tandem construct was performed to monitor autophagic flux as previously reported [26,28]. Transfection of the RFP-GFP-LC3 tandem construct enables detection of autophagosomes as yellow puncta (labeling by signals of both REP and GFP) and autolysosomes as red puncta (signal of RFP alone after quenching of the GFP signal by acidic pH). Using fluorescence microscopy, images were captured at 1, 4, and 8 h after the addition of each pharmacological agent. For each sample, 40 images were taken at a magnification of 630×, and areas of yellow or red puncta were quantified by pixel counts after cutting off background fluorescence using a threshold value.

Assessment of the localization of TFEB: Cells were fixed with 4% paraformaldehyde after pretreatment with a vehicle, TNF/zVAD, rapamycin, TNF/zVAD + rapamycin, Ku-0063794, TNF/zVAD + Ku-0063794, necrostatin-1 or TNF/zVAD + necrostatin-1 for 4 h. The cells were then washed with PBS, blocked with 3% BSA and 0.1% Triton in PBS for 30 min, and incubated overnight in PBS containing 3% BSA and anti-TFEB antibodies (Proteintech, Rosemont, IL). The bound antibodies were labeled with an Alexa Fluor(R) 488 anti-rabbit secondary antibody. For each sample, 50 images were taken at a magnification of 630× using confocal microscopy, and areas of nuclear or cytosolic TFEB were quantified by pixel counts after cutting off background fluorescence using a threshold value.

To quantify the total volume of lysosomes, H9c2 cells were stained with Lysotracker Red (50 nM) for 5 min and visualized using fluorescence microscopy. Prior to staining with Lysotracker Red, cells were pretreated with a vehicle, TNF/zVAD, rapamycin (10 nM), or TNF/zVAD and rapamycin for 8 h. For each sample, 50 images were taken using confocal microscopy, and areas of Lysotracker Red-staining as percentages of cell areas were quantified by pixel counts after cutting off background fluorescence using a threshold value.

2.7. mRNA quantification

Total RNA was isolated from cells by using an RNeasy Fibrous Tissue Mini Kit (Qiagen, Valencia, CA). First-strand sDNA was synthesized using a SuperScript VILO™ cDNA synthesis Kit (Life Technologies). DNA amplification was performed in StepOne™ (Life Technologies) by using Taqman Universal Master Mix (Applied Biosystems, Inc) and the oligonucleotide primers for rat TNF-α (Rn99999017_m1), rat Atg9 (Rn01442245_g1), rat MCOLN1 (Rn01403276_m1), rat β-actin (Rn00667869_m1, Applied Biosystems, Inc.). All assays were performed in duplicate and by the standard curve method using serial cDNA dilution.

2.8. Tissue sampling from myocardial ischemia/reperfusion in vivo for biochemical analyses

Tissue sampling in a rat model of myocardial ischemia/reperfusion *in vivo* was performed as in our previous studies with slight modifications [29]. In brief, male Sprague-Dawley (SD) rats (10 to 12 weeks old) were anesthetized with pentobarbital sodium (80 mg/kg, intraperitoneal injection) and ventilated with a Harvard Model 683 respirator (Harvard Apparatus, South Natick, NA). The chest was opened via a left thoracotomy, and a coronary snare was prepared around the left main coronary artery. A saline-filled catheter was inserted into a carotid artery for monitoring for blood pressure. The catheter placed in the carotid artery was connected into a Nihon-Kohden SCK-590 pressure transducer. An electrocardiogram was recorded by precordial bipolar electrodes. Rectal temperature was adjusted within 37.5 °C–38.5 °C by using a heating lamp when necessary. After 30 min of stabilization, rats underwent 20 min of left coronary artery occlusion and 5 min of reperfusion, and the vehicle (DMSO) or rapamycin (1 mg/kg) was administered intravenously at 5 min before reperfusion. Myocardial ischemia and reperfusion were confirmed by the appearance of regional cyanosis and ST segment elevation on an electrocardiogram and visible hyperemia on the ventricular surface, respectively. At 5 min after reperfusion, hearts were excised, immediately soaked in ice-cold saline, quickly mounted onto a Langendorff apparatus, and perfused with ice-cold saline to wash out blood. The coronary artery was re-occluded and Evans blue dye was infused into the aorta to negatively mark the area at risk, from where myocardial tissue was quickly sampled and frozen in liquid nitrogen. The frozen tissues were stored at −80 °C until use for immunoprecipitation or immunoblotting. Frozen heart samples were homogenized in ice-cold buffer (CelLytic™ MT Cell Lysis Reagent) including 0.5 mmol/L Na_3VO_4, a protease inhibitor cocktail (Complete mini, Roche Molecular Biochemicals, Mannheim, Germany), and 1 mmol/l phenylmethylsulfonyl fluoride. The homogenate was centrifuged at 13,000*g* for 15 min to obtain the supernatant for western blotting and immunoprecipitation.

2.9. Statistical analysis

Data are presented as means ± standard error of the mean. One-way analysis of variance (ANOVA) was used to detect significant differences between group means in the treatment groups. When ANOVA indicated a significant overall difference, multiple comparisons of the groups were performed by the Tukey *post-hoc* test. A difference was considered to be statistically significant if p was < 0.05. All of above statistical analyses were performed using EZR software (Jichi Medical University, Saitama, Japan).

3. Results

3.1. TNF/zVAD induced RIP1/RIP3/MLKL-dependent cell death in H9c2 cells

Treatment with TNF-α alone induced cleavage of RIP1 and caspase-3, and addition of zVAD to TNF-α (TNF/zVAD) prevented TNF-α-induced cleavage of RIP1 and caspase-3 (Supplemental Fig. 1A, B). TNF/zVAD increased LDH release from 3.4 ± 1.3% in the vehicle-treated control to 46.1 ± 2.3% (Supplemental Fig. 1C). TNF/zVAD-induced cell death was suppressed by necrostatin-1 (5.9 ± 0.9%), a RIP1 inhibitor (Supplemental Fig. 1C). The effect of RIP1 inhibition on TNF/zVAD-induced cell death was mimicked by siRNA-mediated knockdown of RIP3 or MLKL (Supplemental Fig. 1D, E). These results confirmed that TNF/zVAD induces necroptosis through a RIP1/RIP3/MLKL-dependent pathway in H9c2 cells. Induction of necroptosis by TNF/zVAD was confirmed in neonatal rat cardiomyocytes as well (Supplemental Fig. 2).

3.2. mTORC1 inhibition suppressed necroptosis through a p70s6K-independent pathway

Rapamycin, an allosteric mTORC1 inhibitor, reduced phosphorylation of p70s6K and S6 but preserved phosphorylation of Akt-Ser473, a downstream target of mTORC2 (Fig. 1B). On the other hand, Ku-0063794, an ATP-competitive mTOR inhibitor, reduced Akt-Ser473 phosphorylation together with reduction in the phosphorylation levels of p70s6K and S6 (Fig. 1B). Treatment with rapamycin reduced TNF/zVAD-induced cell death from 45.0 ± 1.3% in the vehicle-treated control to 22.8 ± 1.3% (Fig. 1C) as did in a previous study [26]. Ku-0063794 mimicked the effect of rapamycin on TNF/zVAD-induced cell death (23.5 ± 1.4%), indicating that inhibition of mTORC1 but not inhibition of mTORC2 attenuates necroptosis. In contrast, inhibition of p70s6K activity by PF-4708671 had no effect on TNF/zVAD-induced cell death (44.8 ± 1.9%). Thus, the cytoprotective effect of mTORC1 inhibition is unlikely to be mediated by suppression of p70s6K activity.

3.3. Protective effect of mTORC1 inhibition on necroptosis was not mediated by regulators upstream of RIP1 activation

To examine whether the transition process from TNF receptor activation to formation of complex IIa is modulated by mTORC1 inhibition, we first determined protein levels of components involved in the canonical TNF-triggered necroptotic pathway. However, there were no significant changes by rapamycin in protein levels of TRAF2, transforming growth factor β-activated kinase 1 [TAK1], I kappa B kinase β [IKKβ], cIAP, A20, and cylindromatosis [CYLD] or necrosome components (FADD, caspase-8, RIP3, and MLKL) as shown in Supplemental Figs. 3–5. The extent of TNF-induced RIP1 cleavage was not changed by rapamycin, indicating that transition from complex I to complex IIa was not modulated. Treatment with TNF or TNF/zVAD induced modest phosphorylation of p38MAPK and significant phosphorylation of p65, indexes of TAK1 and NFκB activity, respectively (Supplemental Figs. 3–5). Rapamycin did not modulate TNF or TNF/zVAD-induced p38MAPK phosphorylation but significantly reduced p65 phosphorylation 4-h after stimulation with TNF or TNF/zVAD. Since an earlier study showed that RIP1 activation increased TNF transcription, which was exaggerated in the presence of zVAD [30], we postulated that upregulation of autocrine TNF production might be suppressed by mTORC1 inhibition. However, this possibility was excluded by the finding that rapamycin did not reduce TNF/zVAD-induced elevation of TNF mRNA level (Supplemental Fig. 6).

Next, we examined whether increased activity of endogenous necroptosis suppressors (TAK1, IKKα/β, and/or cIAP) is involved in the protective effect of mTORC1 inhibition. Doses of 5s7, a TAK1 inhibitor, were selected according to results of pilot experiments (Supplemental Fig. 7). Doses of TPCA-1, an IKKα/β inhibitor, and BV6, a cIAP inhibitor, were selected according to the reported IC50 values and results of a previous study [11]. Addition of 5s7, TPCA-1, and BV6 to TNF/zVAD exaggerated TNF/zVAD-induced cell death, indicating that TAK1, IKKα/β, and cIAP serve as endogenous suppressors of canonical TNF-induced necroptosis also in H9c2 cells, but the agents did not abolish protection afforded by rapamycin (Fig. 2A–C).

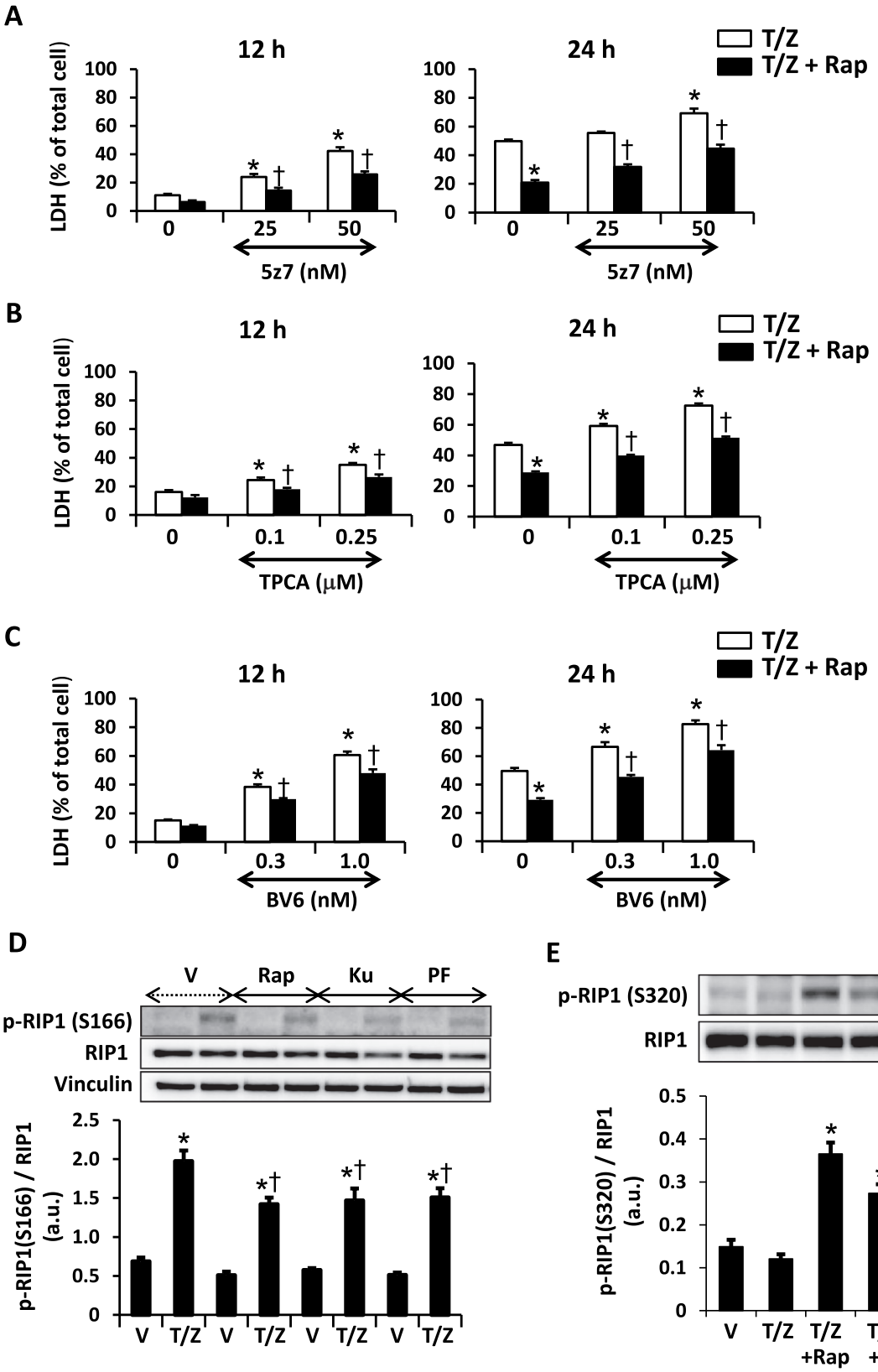

Fig. 2. Effects of inhibitors of endogenous necroptosis suppressors upstream of RIP1 on rapamycin-induced protection and effects of mTOR and p70s6K inhibitors on phosphorylation of RIP1.

(A–C) Effects of 5z7 (A), a TAK1 inhibitor, TPCA-1 (B), an IKKα/β inhibitor, and BV6 (C), a cIAP inhibitor, on rapamycin-induced protection from T/Z-induced cell death. V = vehicle, T/Z = TNF-α and zVAD, Rap = rapamycin. N = 5 in each group. *$p < 0.05$ vs. V. $^{\dagger}p < 0.05$ vs. T/Z. (D) Effects of mTOR inhibitors (Rap, Ku) and a p70s6K inhibitor (PF) on T/Z-induced RIP1-Ser166 phosphorylation. Representative Western blots and summarized data are shown. Ku = Ku-0063794, PF = PF-4708671. N = 5 in each group. *$p < 0.05$ vs. V. $^{\dagger}p < 0.05$ vs. T/Z + V. (E) Effects of mTOR inhibitors (Rap, Ku) and a p70s6K inhibitor (PF) on RIP1 phosphorylation at Ser320 in T/Z-treated cells. Representative Western blots and summarized data are shown. N = 4 in each group. *$p < 0.05$ vs. T/Z. $^{\dagger}p < 0.05$ vs. T/Z + Rap.

3.4. Inhibition of mTORC1 partially blocked TNF/zVAD-induced RIP1-Ser166 phosphorylation but increased phosphorylation of RIP1-Ser320, an inhibitory phosphorylation site

Since previous studies showed that the extent of RIP1-Ser166 phosphorylation, an autophosphorylation site in the RIP1 kinase domain, positively correlates with RIP1 activity [31,32], we examined the effect of mTORC1 inhibition on TNF/zVAD-induced RIP1-Ser166 phosphorylation. TNF/zVAD increased RIP1-Ser166 phosphorylation by 3.4 fold compared with its vehicle control, which was completely blocked by treatment with necrostatin-1 (Supplemental Fig. 8). mTORC1 inhibition by rapamycin or Ku-0063794 and inhibition of p70s6K by PF-4708671 modestly reduced RIP1-Ser166 phosphorylation (Fig. 2D), indicating that mTORC1/p70s6K pathway partly regulates RIP1-Ser166 phosphorylation. Since PF-4708671 failed to protect cells from TNF/zVAD-induced necroptosis (Fig. 1C), the results suggest that modest reduction in RIP1-Ser166 phosphorylation is insufficient for explaining the protection afforded by mTORC1 inhibition.

In contrast to the role of RIP1-Ser166, serine residues in the intermediate domain of RIP1 have been reported to negatively regulate RIP1 activity [12,33–37]. Three serine residues were identified as IKKα/β-mediated inhibitory phosphorylation sites on RIP1 [34], one of which is human RIP1-Ser416 (rat RIP1-Ser414). Phosphorylation of Ser320 or Ser336 in RIP1 has been reported to contribute to the suppression of RIP1 activity by activation of MAPK-activated protein kinase 2 (MK2) and reduction in TNF-induced cell death [35–37]. These serine residues exist on the RXX(S*/T*) motif of the amino acid sequence of rat RIP1. Using an antibody that detects phosphorylation of Ser/Thr in the RXX (S*/T*) motif [38], we examined the effect of mTORC1 inhibition on phosphorylation of RXX(S*/T*) motif in RIP1. p-RXX(S*/T*) signals in the RIP1 immunoprecipitates were detected in the vehicle controls, which were not modified by TNF/zVAD (Supplemental Fig. 9A). Rapamycin and Ku-0063794, but not PF-4708671, increased p-RXX(S*/T*) signals in the RIP1 immunoprecipitates in TNF/zVAD-treated cells (Supplemental Fig. 9A–B). Such an effect of rapamycin on RIP1-RXX (S*/T*) phosphorylation signals after TNF/zVAD treatment was observed in cells transfected with RIP1-WT, RIP1-S414A and RIP1-S335A, but not in cells transfected with RIP1-S320A (Supplemental Fig. 9C). Western blottings using p-Ser320-RIP1 specific antibody showed that rapamycin and Ku-0063794, but not PF-4708671, increased RIP1-Ser320 phosphorylation in total cell lysates (Fig. 2E) and RIP1 immunoprecipitates (Supplemental Fig. 10) of TNF/zVAD-treated cells.

Rapamycin reduced RIP1-RIP3 binding after TNF/zVAD treatment (Fig. 3A), and its effect on RIP1-RIP3 interaction was mimicked by Ku-0063794 but not by PF-4708671 (Fig. 3B). TNF/zVAD similarly increased interaction of RIP1-WT with RIP3 and interaction of RIP1-S320A with RIP3 (Fig. 3C–D). However, rapamycin failed to suppress TNF/zVAD-induced increase in RIP3-RIP1-Ser320A interaction (Fig. 3D). The findings suggest that phosphorylation of RIP1 at Ser320 is necessary for rapamycin to significantly suppress TNF/zVAD-induced RIP1-RIP3 binding.

3.5. mTORC1 inhibition failed to prevent necroptosis of cells with RIP1-S320A

To examine the role of RIP1-Ser320 phosphorylation in cytoprotection, we compared the effects of mTORC1 inhibition on necroptosis in RIP1-WT-expressed cells and RIP1-S320A-expressed cells. Although the transfection efficiencies of RIP1 plasmids were low (20–40%), suppression of LDH release after TNF/zVAD by rapamycin was significantly attenuated in RIP1-S320A-transfected cells compared with LDH release in RIP1-WT-transfected cells (Fig. 4). To examine whether RIP1-S320 phosphorylation is sufficient for protection from necroptosis, RIP1-S320D was transfected into H9c2 cells. LDH release after TNF/zVAD treatment in RIP1-320D-transfected cells was not significantly different from that in RIP1-WT-transfected cells (Fig. 4), suggesting that phosphorylation of RIP1-Ser320 alone is insufficient for prevention of necroptosis. Rapamycin suppressed TNF/zVAD-induced cell death in cells expressing RIP1-Ser320D to an extent similar to that in cells expressing RIP1-WT. Since rapamycin induced reduction in RIP1-Ser166 phosphorylation (Fig. 2D) together with increase in RIP1-Ser320 phosphorylation (Fig. 2E), it is likely that both Ser320 phosphorylation and Ser166 dephosphorylation in RIP1 are important for mTORC1 inhibition to achieve significant RIP1 inactivation and cytoprotection from necroptosis.

3.6. Like rapamycin treatment, RIP1 inhibition relieved TNF/zVAD-induced suppression of autophagy

In a previous study [26], we found that TNF/zVAD and bafilomycin A1 increased LC3-II levels to comparable levels and that the combination of TNF/zVAD and bafilomycin A1 did not further increase LC3-II level. Using a tandem RFP-GFP-LC3 reporter, we showed the time-course of numbers of autophagosomes and autolysosomes after TNF/zVAD treatment, which indicated suppression of autophagic flux by TNF/zVAD and restoration of autophagic flux by rapamycin [26] In the present study, we confirmed the effects of TNF/zVAD with and without bafilomycin A1 on LC3-II protein level (Supplemental Fig. 11) and the effects of TNF/zVAD and rapamycin on autophagic flux by using a tandem RFP-GFP-LC3 construct; rapamycin increased both autophagosomes (yellow puncta) and autolysosomes (red puncta) with a reduced autophagosome-to-autolysosome ratio, indicating increase in autophagic flux, and that TNF/zVAD increased autophagosomes and autolysosomes without a reduction in the autophagosome-to-autolysosome ratio (Fig. 5A–C). Necrostatin-1, RIP1 inhibitor, mimicked the effect of rapamycin on the autophagosome-to-autolysosome ratio in TNF/zVAD-treated cells, while necrostatin-1 had no effect on autophagic flux in vehicle-treated cells (Fig. 5A–C). In contrast to necrostain-1, RIP3 knockdown had no effect on the number of autophagosomes and autolysosomes or the autophagosome-to-autolysosome ratio in TNF/zVAD-treated cells (Supplemental Fig. 12). Together with the findings indicating inactivation of RIP1 by mTORC1 inhibition (Figs. 2 and 3), the results suggest that inhibition of RIP1 activity, not inhibition of RIP1-RIP3 interaction, by rapamycin relieves TNF/zVAD-induced suppression of autophagic flux.

3.7. TNF/zVAD reduced nuclear TFEB level, and the effect of TNF/zVAD was prevented by inhibition of RIP1 or mTORC1

Since our previous study [26] showed that impaired autophagy by TNF/zVAD was associated with suppressed fusion of autophagosomes with lysosomes, we examined the possibility that TFEB, a master regulator of lysosome biogenesis, is modified by activation of necroptotic signals. In vehicle-treated H9c2 cells, approximately 40% of TFEB signals were detected in the nucleus, and TNF/zVAD significantly reduced nuclear TFEB (Fig. 6A, B). Necrostatin-1 preserved the nuclear TFEB level in TNF/zVAD-treated cells (Fig. 6A, B). Inhibition of mTORC1 by rapamycin or Ku-0063794 enhanced nuclear TFEB signals both with and without TNF/zVAD treatment (Fig. 6C, D). Nuclear translocation of TFEB by inhibition of mTORC1 or RIP1 in TNF/zVAD-treated cells was confirmed by determination of TFEB proteins in cytosolic and nuclear fractions (Fig. 6E). Interestingly, TNF/zVAD increased phosphorylation of ERK1/2, which was inhibited by necrostatin-1 (Supplemental Fig. 13). The mRNA levels of Atg9b and mucolipin 1 (MCOLN1), TFEB target genes, were comparable in TNF/zVAD-treated cells and vehicle-treated cells, but treatment with rapamycin or necrostatin-1 significantly increased the level of MCOLN1 mRNA in TNF/zVAD-treated cells (Supplemental Fig. 14). In addition, treatment with rapamycin increased the total volume of lysosomes as shown by areas stained with Lysotracker Red in vehicle- and TNF/zVAD-treated cells (Fig. 7).

3.8. Knockdown of TFEB expression prevented the protective effects of RIP1 inhibition on autophagy and necroptosis in TNF/zVAD-treated cells

The effect of suppression of TFEB protein level on autophagic flux with and without RIP1 inhibition was examined by using the tandem

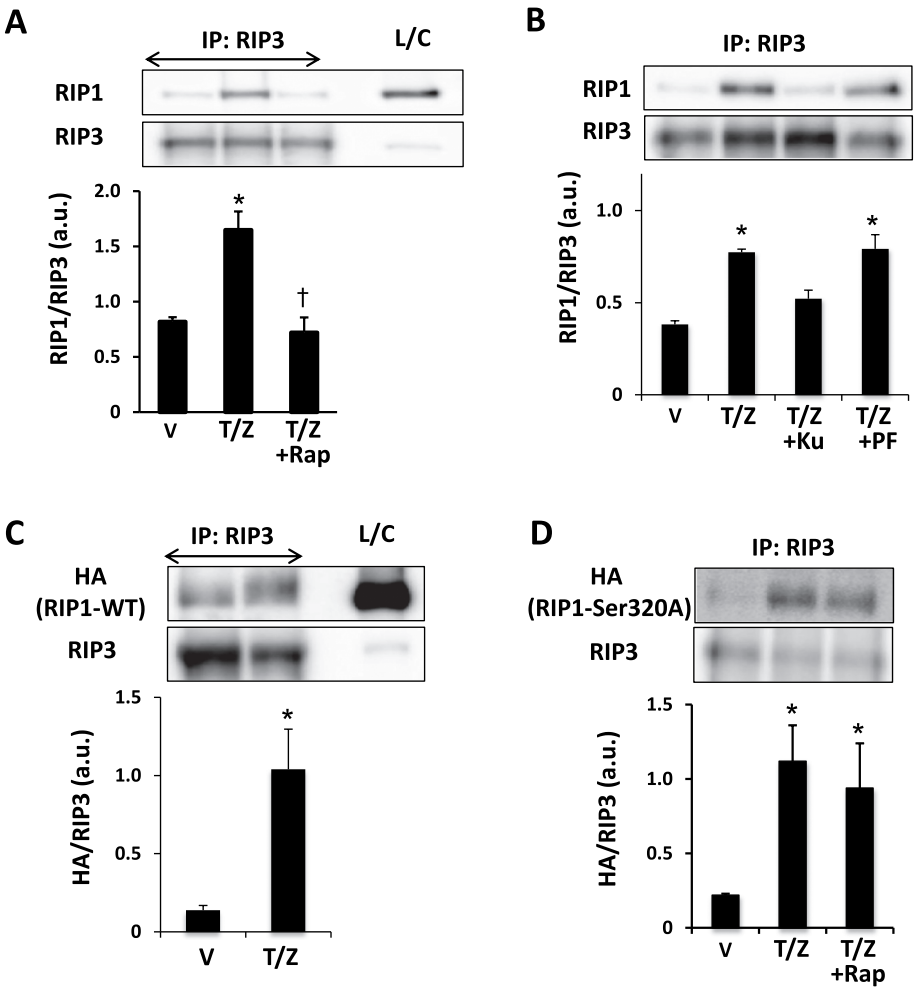

Fig. 3. Effects of mTOR inhibitors and a p70s6K inhibitor on RIP1-RIP3 interaction in cells treated with TNF/zVAD.
Representative immunoblots and group means are shown. (A) RIP1-RIP3 interaction in vehicle-treated and TNF/zVAD-treated cells. N = 4 in each group. V = vehicle, T/Z = TNF-α and zVAD, Rap = rapamycin. *p < 0.05 vs. V. †p < 0.05 vs. T/Z. L/C = lysate control. (B) RIP1-RIP3 interaction in cells treated with TNF/zVAD alone, TNF/zVAD and Ku-0063794, and TNF/zVAD and PF-4708671. N = 4 in each group. V = vehicle, T/Z = TNF-α and zVAD, Ku = Ku-0063794, PF = PF-4708671. *p < 0.05 vs. V. (C) RIP1-RIP3 interaction in cells transfected with HA-RIP1-WT (RIP1-WT). N = 3 in each group. *p < 0.05 vs. V. L/C = lysate control. (D) Effect of rapamycin on RIP1-RIP3 interaction in cells transfected with HA-RIP1-Ser320A (RIP1-S320A). N = 3 in each group. *p < 0.05 vs. V.

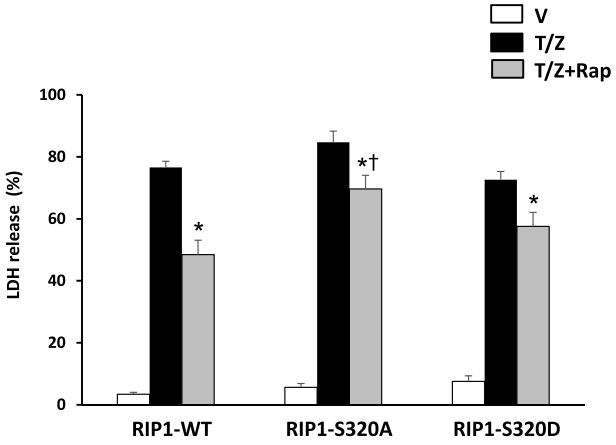

Fig. 4. Role of RIP1-S320 phosphorylation in rapamycin-induced suppression of necroptosis.
LDH release into the culture medium as a percentage of total cellular LDH activity is shown. Cells were transfected with the HA-RIP1-WT plasmid (RIP1-WT), HA-RIP1-Ser320A (RIP1-S320A) or HA-RIP1-Ser320D (RIP1-S320D) 24 h before treatment with a vehicle (V), TNF/zVAD (T/Z), or TNF/zVAD + rapamycin (T/Z + Rap) for 24 h. N = 6 in each group. *p < 0.05 vs. V. †p < 0.05 vs. T/Z + Rap-treated cells transfected with RIP1-WT.

RFP-GFP-LC3 construct. Inhibition of RIP1 by necrostatin-1 increased autolysosomes and significantly reduced the autophagosome-autolysosome ratio after TNF/zVAD treatment in control siRNA transfected cells (Fig. 8A–D). However, such effects of necrostatin-1 were not detected in TFEB siRNA-transfected cells. Results of Western blotting analyses for LC3-II showed that LC3-II accumulation induced by TNF/zVAD was prevented by necrostatin-1 and that such an effect of necrostatin-1 was lost in TFEB siRNA-transfected cells (Supplemental Fig. 15). TFEB knockdown inhibited rapamycin-induced restoration of autophagic flux in TNF/zVAD-treated cells also (Supplemental Fig. 16). TFEB knockdown did not affect the extent of TNF/zVAD-induced cell death, but it significantly attenuated the protective effect of rapamycin on necroptosis (Fig. 8E). These findings indicate that TFEB is indispensable for mTORC1 inhibition-induced restoration of autophagic flux and suppression of necroptosis.

3.9. Rapamycin suppressed TNF/zVAD-induced p53 upregulation, but p53 was dispensable for TNF/zVAD-induced necroptosis

Treatment with TNF and treatment with TNF/zVAD increased the p53 protein level in H9c2 cells by 1.6 or 1.8 fold, respectively, and rapamycin suppressed increase in the p53 protein level by TNF/zVAD (Supplemental Fig. 17). However, the extent of TNF/zVAD-induced cell death was not changed by interventions that downregulate or upregulates p53 activity (Supplemental Figs. 18 and 19).

3.10. Rapamycin increased RIP1-Ser320 phosphorylation in hearts in vivo

Inhibition of mTORC1 or RIP1 upon reperfusion has been shown to limit myocardial infarct size after ischemia/reperfusion in vivo [7,8,39,40]. Thus, we examined whether rapamycin increases RIP1-Ser320 phosphorylation in rat hearts. Tissues were sampled from left

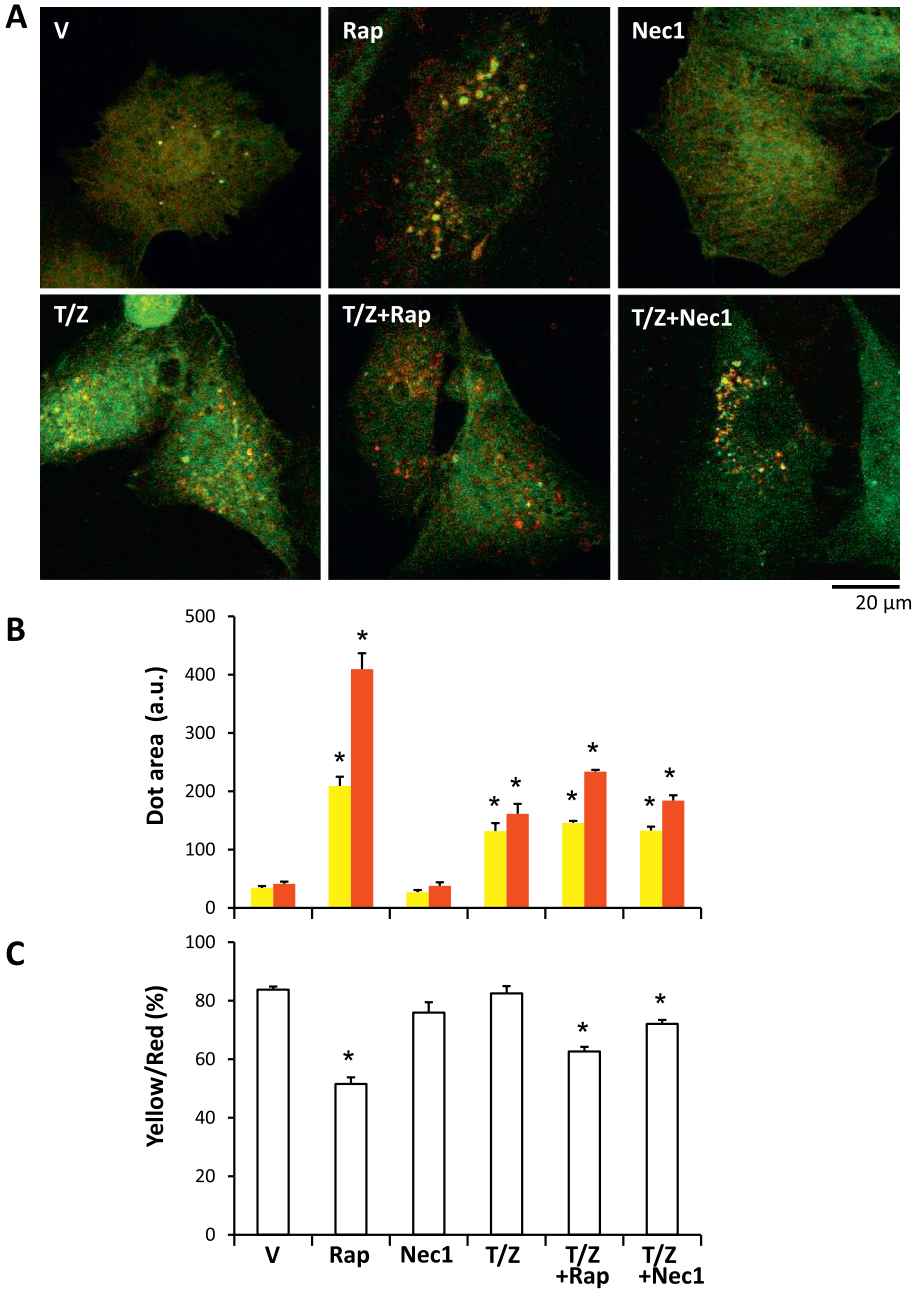

Fig. 5. Autophagic flux assessed by tandem RFP-GFP-LC3.
(A) Representative images of H9c2 cells transfected with tandem RFP-GFP-LC3 plasmids at 4 h after pharmacological treatments (magnification 630×). V = vehicle, Rap = rapamycin, Nec1 = necrostatin-1, T/Z = TNF-α and zVAD. (B) Group mean data for images captured 4 h after the addition of each drug. Areas of yellow puncta (autophagosomes) and red puncta (autolysosomes) were quantified. N = 15 in each group. a.u. = arbitrary units. *p < 0.05 vs. V. (C) Group mean data for the ratio of yellow puncta area to red puncta area. *p < 0.05 vs. V.

ventricular regions subjected to 20-min ischemia/5-min reperfusion *in vivo* for Western blotting. Administration of rapamycin at 5 min before reperfusion significantly increased RIP1-Ser320 phosphorylation by almost twofold in the myocardium (Supplemental Fig. 20).

4. Discussion

There are three salient findings in the present study. First, we found a novel mTORC1-mediated RIP1 regulation, i.e., inhibition of RIP1-Ser320 phosphorylation, and its major role in modulation of necroptosis. Second, we obtained circumstantial evidence that the lysosome is a major target for mTORC1 inhibition to restore autophagy from its impairment by necroptotic signals. Third, we showed that mTORC1 inhibition is a distinct protective strategy from strategies to inhibit necroptosis signals upstream of RIP1 and to inhibit p53 upregulation.

Kinase activity of RIP1 is mainly regulated by post-transcriptional modification on its kinase domain [41]. Degterev et al. identified Ser14/15, Ser20, Ser161, and Ser166 as autophosphorylation sites of RIP1 [31]. The extent of RIP1-Ser166 phosphorylation positively correlates with RIP1 activity [32]. In addition, phosphorylation of Ser in the intermediate domain of RIP1 has been shown to negatively modulate RIP1-dependent cell death [12,33]. Furthermore, recent studies have shown that MK2 directly phosphorylates RIP1 at Ser320, leading to suppression of TNF-mediated apoptosis and necroptosis [35–37]. In the present study, mTORC1 inhibitors and a p70s6 kinase inhibitor, PF-

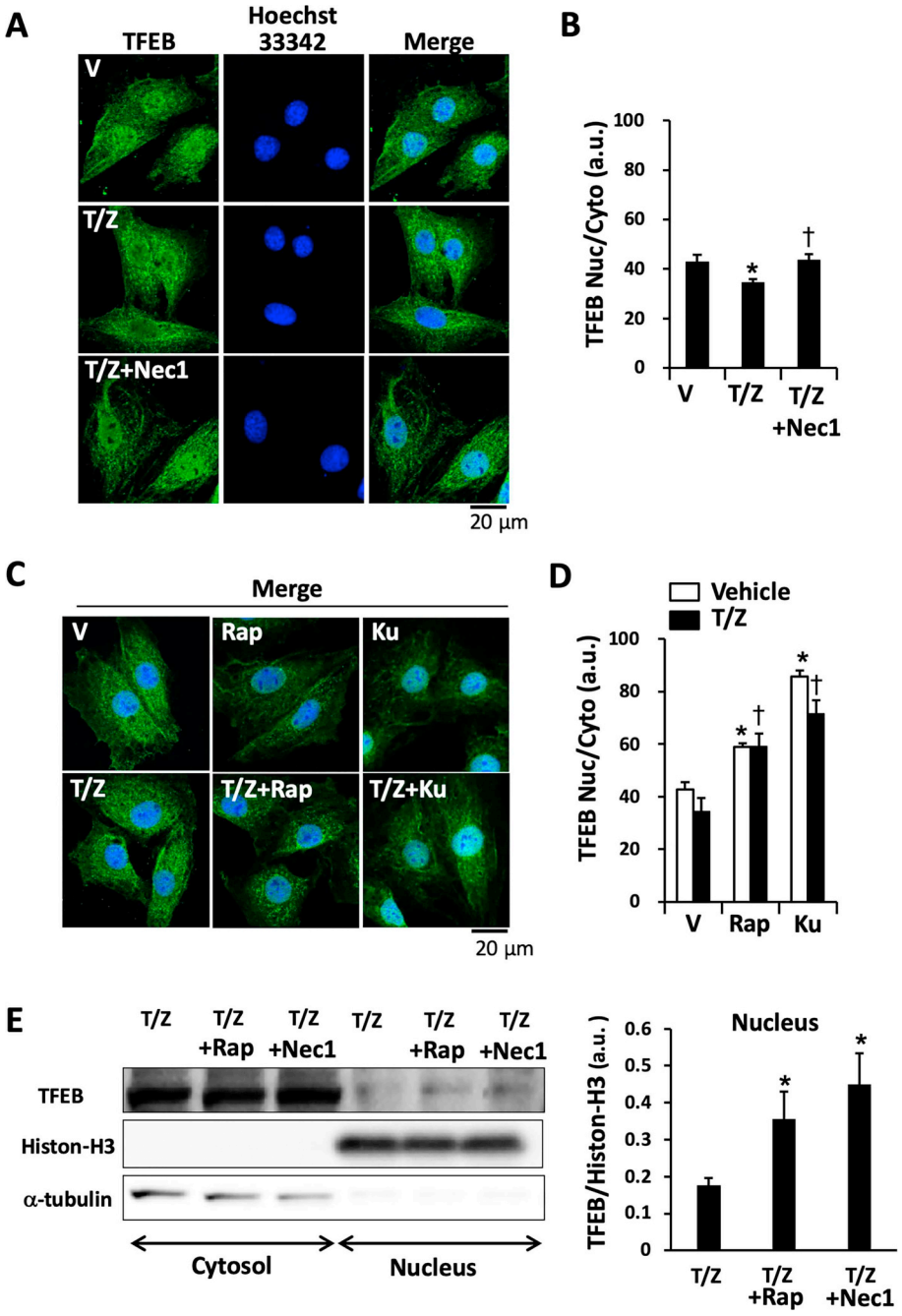

Fig. 6. Effects of TNF/zVAD, RIP1 inhibition and mTORC1 inhibition on intracellular localization of TFEB.

(A, C) Representative images of H9c2 cells stained with anti-TFEB antibodies and Hoechst 33342 at 4 h after pharmacological treatments (magnification 630×). V = vehicle, Rap = rapamycin, Ku = Ku-0063794, T/Z = TNF-α and zVAD, Nec1 = necrostatin-1. (B, D) Group mean data for the ratio of nuclear TFEB to cytosolic TFEB. Anti-TFEB antibody-positive area was quantified by using Image J. N = 45–55 in each group. a.u. = arbitrary units. *p < 0.05 vs. cells treated with a vehicle of T/Z and a vehicle of Rap and Ku. †p < 0.05 vs. cells treated with T/Z and a vehicle of Rap and Ku. (E) Representative immunoblots for TFEB protein in cytosolic and nuclear fractions and summarized data for TFEB in nuclear fractions. Histon-H3 and α-tubulin were used as loading controls of nuclear and cytosolic fractions, respectively. N = 4 in each group. *p < 0.05 vs. T/Z.

4708671, similarly reduced RIP1-Ser166 phosphorylation (Fig. 2D), while mTORC1 inhibitors, but not PF-4708671, protected cells from necroptosis (Fig. 1C). Thus, we postulated an additional mechanism for mTORC1 inhibitors to inhibit RIP1 activity and examined effects of mTORC1 inhibition on the intermediate domain of RIP1. Signals for p-RXX(S*/T*) in RIP1 immunoprecipitates were significantly increased by mTORC1 inhibitors but not by PF-4708671 (Supplemental Fig. 9A, B), and experiments using mutants of RIP1-Ser320, 335 and/or 414 revealed that increased phosphorylation at Ser320 in RIP1 was responsible for increased signals of the p-RXX(S*/T*) motif of RIP1 by mTORC1 inhibition (Supplemental Fig. 9C). RIP1 phosphorylation at Ser320 by rapamycin and Ku-0063794, but not by PF-4708671, in TNF/zVAD-treated cells was confirmed by the use of antibodies that specifically detect RIP1 phosphorylation at Ser320 (Fig. 2E and Supplemental Fig. 10). Furthermore, rapamycin failed to protect cells expressing HA-RIP1-S320A from necroptosis (Fig. 4). On the other hand, there was no significant difference in the extent of TNF/zVAD-induced cell death between cells expressing RIP1-WT and those expressing RIP1-S320D (Fig. 4), suggesting that phosphorylation of RIP1-Ser320 alone is not sufficient for protection from TNF/zVAD-induced cell death. Taken together, the findings suggest that both Ser320 phosphorylation and Ser166 dephosphorylation in RIP1 are important for mTORC1 inhibition to achieve significant RIP1 inactivation and cytoprotection from necroptosis.

A few possibilities can be speculated for the mechanism by which mTORC1 inhibition increased phosphorylation of RIP1-Ser320. First, IKKα/β might mediate phosphorylation at the intermediated domain of RIP1. Dondelinger et al. showed that IKKα/β-mediated RIP1 phosphorylation preserves RIP1 in complex I after TNF receptor activation, leading to protection from RIP1-dependent apoptosis/necroptosis [33]. Three serine residues (Ser166, Ser331, and Ser416 in the rat) were identified as IKKα/β-mediated putative phosphorylation sites on RIP1

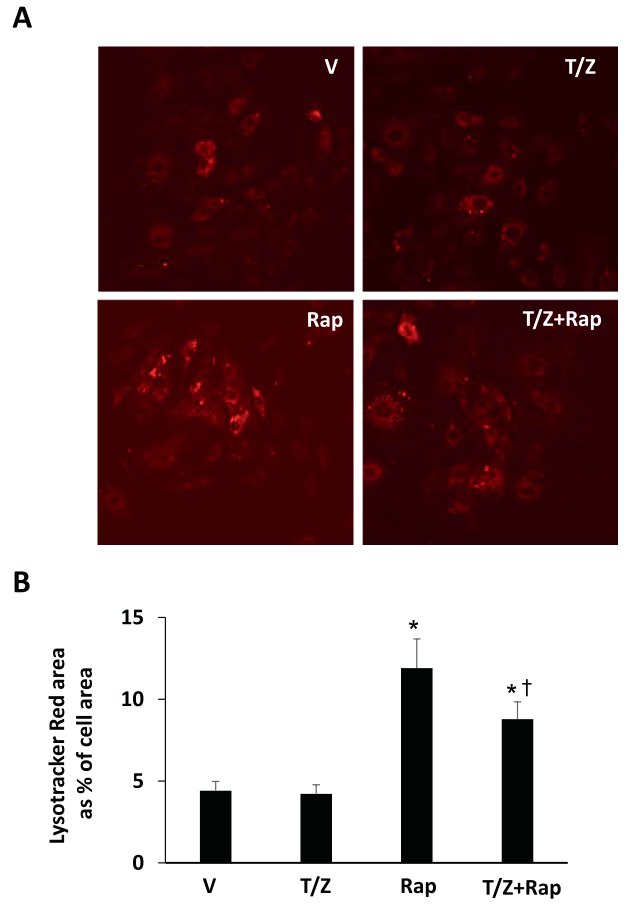

Fig. 7. Effects of rapamycin on lysosome volume in TNF/zVAD-treated cells. (A) Representative images of H9c2 cells stained with Lysotracker Red at 4 h after pharmacological treatments (magnification 200×). V = vehicle, T/Z = TNF-α and zVAD, Rap = rapamycin. (B) Group mean data for Lysotracker Red-stained area as % of total cell area in images captured 4 h after the addition of each drug. *p < 0.05 vs. V. †p < 0.05 vs.Rap.

[34]. However, mTORC1 inhibition actually suppressed TNF/zVAD-mediated enhancement in IKKα/β activity (Supplemental Figs. 3–5), arguing against the possibility that IKKα/β contributed to mTORC1 inhibition-mediated RIP1-Ser320 phosphorylation. Second, MK2, which directly phosphorylates RIP1 at Ser320 [35–37], might be modulated by mTORC1 inhibition, though a study showed that mTORC1 inhibitors downregulated translation of MK2 [42]. By the use of MALDI-TOF/MS in *post hoc* experiments, we identified heat shock protein (Hsp) 27 in the RIP1 immunoprecipitates. Hsp27 has been reported to interact with MK2 [43,44], and MK2 and Hsp27 have several proline-directed sites potentially phosphorylated by mTOR complexes. Thus, there is the possibility that mTORC1 inhibition-induced changes in activity of MK2 and Hsp27 or affinity of MK2-Hsp27-RIP1 complex modulate phosphorylation of RIP1 at Ser320. Third, TORC1 inhibition might modulate the sensitivity of RIP1-Ser320 to its upstream signals by a change in the p62-RIP1 interaction. In a previous study, we observed that rapamycin significantly inhibited TNF/zVAD-induced complex formation of p62 and RIP1 ([26], Fig. 9). A p62 binding site (Lys377) and Ser320 in RIP1 are close [41], and prevention of p62 binding to RIP1 by mTORC1 inhibition might therefore change the sensitivity of Ser320 to its upstream signals (Fig. 9). Nevertheless, further investigation is necessary for clarifying the mechanism of RIP1 inactivation by mTORC1 inhibition.

Following up a previous study [26], we searched for the mechanism by which mTORC1 inhibition improved autophagy in cells with activated necroptotic signals. Multiple steps of autophagic flux are regulated by mTORC1 [45,46]. mTORC1 suppresses ULK1 activation by phosphorylating ULK1-Ser757, leading to disruption of the ULK1-AMPK complex [47]. mTORC1 inhibits transcriptional activity of TFEB, a master gene of lysosome biogenesis [48], by phosphorylation at Ser142 and Ser211, which promotes its cytoplasmic localization [49,50]. ERK is also reported to regulate TFEB function by phosphorylation of TFEB at Ser142 [49]. Interestingly, Yonekawa et al. [27] recently reported that siRNA-mediated knockdown of RIP1 reduced ERK activity, leading to acceleration of autophagic flux through TFEB-mediated upregulation of lysosomal function.

Consistent with the findings by Yonekawa et al. [27], the effect of an mTORC1 inhibitor on autophagic flux in TNF/zVAD-treated cells was mimicked by a pharmacological inhibitor of RIP1 (Fig. 5, Supplemental Fig. 15). Furthermore, TNF/zVAD increased phosphorylation of ERK1/2, which was abolished by necrostatin-1 (Supplemental Fig. 13). An increase in nuclear TFEB by mTORC1 inhibition was observed not only in normal cells but also TNF/zVAD-treated cells (Fig. 6). Furthermore, increased levels of nuclear TFEB by rapamycin and by necrostatin-1 were associated with upregulated expression of mucolipin 1, a key lysosomal Ca^{2+} channel, that controls both lysosomal biogenesis and reformation (Supplemental Fig. 14) and with increase in lysosome volume (Fig. 7). On the other hand, involvement of activated TAK1 and IKK complex [51–53] is unlikely to be involved in promotion of autophagy by mTORC1 inhibition because rapamycin attenuated TNF/zVAD-induced p38MAPK phosphorylation, an index of TAK1 activity, and p65 phosphorylation, an index of IKKα/β activation (Supplemental Figs. 3–5). Taken together, the present findings support the notion that not only ULK1 activation but also RIP1 inhibition, which promotes lysosomal function via TFEB, contributes to restoration of autophagy by mTORC1 inhibition in TNF/zVAD-treated cardiomyocytes.

Suppression of TFEB expression abolished the protective effects of an mTORC1 inhibitor on both autophagy and necroptosis in TNF/zVAD-treated cells (Fig. 8). An important question is whether the restoration of autophagy contributes to the protection against necroptosis. Unfortunately, we could not answer to this question by use of ULK1 knockdown or bafilomycin A1 in the present study, though we previously reported that knockdown of Atg 5 expression significantly attenuated protection afforded by rapamycin against necroptosis [26]. Rapamycin reduced ULK1-Ser757 phosphorylation, which reportedly promotes autophagy by mTORC1 inhibition, but knockdown of ULK1 expression alone tended to suppress TNF/zVAD-induced necroptosis (Supplemental Fig. 21). Bafilomycin A1 at a dose of 100 nM significantly suppressed TNF/zVAD-induced cell death and bafilomycin A1 at doses of 25, 50 and 100 nM did not eliminate the protection afforded by rapamycin (Supplemental Fig. 22). A possible explanation for apparent protection from necroptosis by bafilomycin A1 and ULK1 knockdown is interruption of necroptotic signaling that is mediated by autophagosomal proteins [24,25]. Because of cross-talk between autophagy and necroptosis signaling [24–26], the impact of intervening autophagy on cell death is likely to be different depending on the step at which autophagy intervened. TFEB is known to coordinate cytokine production and regulate mitophagy [54]. In addition, TFEB positively regulates lysosomal exocytosis by induction of MCOLN1 [55], a gene that was significantly upregulated by inhibition of RIP1 and mTORC1 in the present study (Supplemental Fig. 14). Nevertheless, the present findings indicate that TFEB activation is indispensable for mTORC1 inhibition-induced suppression of necroptosis, and further study is necessary for clarifying possible involvement of autophagy-dependent and -independent mechanisms in the protection afforded by activated TFEB.

Since mTORC1 has multiple functions besides regulation of autophagy, we examined the possibility that modification of intracellular signaling upstream of RIP1 by mTORC1 inhibition is involved in the protection of H9c2 cells from necroptosis. Treatment with rapamycin induced no significant changes in the protein levels of regulators upstream of RIP1 (TRAF2, TAK1, IKKβ, cIAP, A20, and CYLD) or in the levels of cleaved RIP1 in TNF-treated cells (Supplemental Figs. 3–5). Furthermore, the protective effect of rapamycin on TNF/zVAD-induced

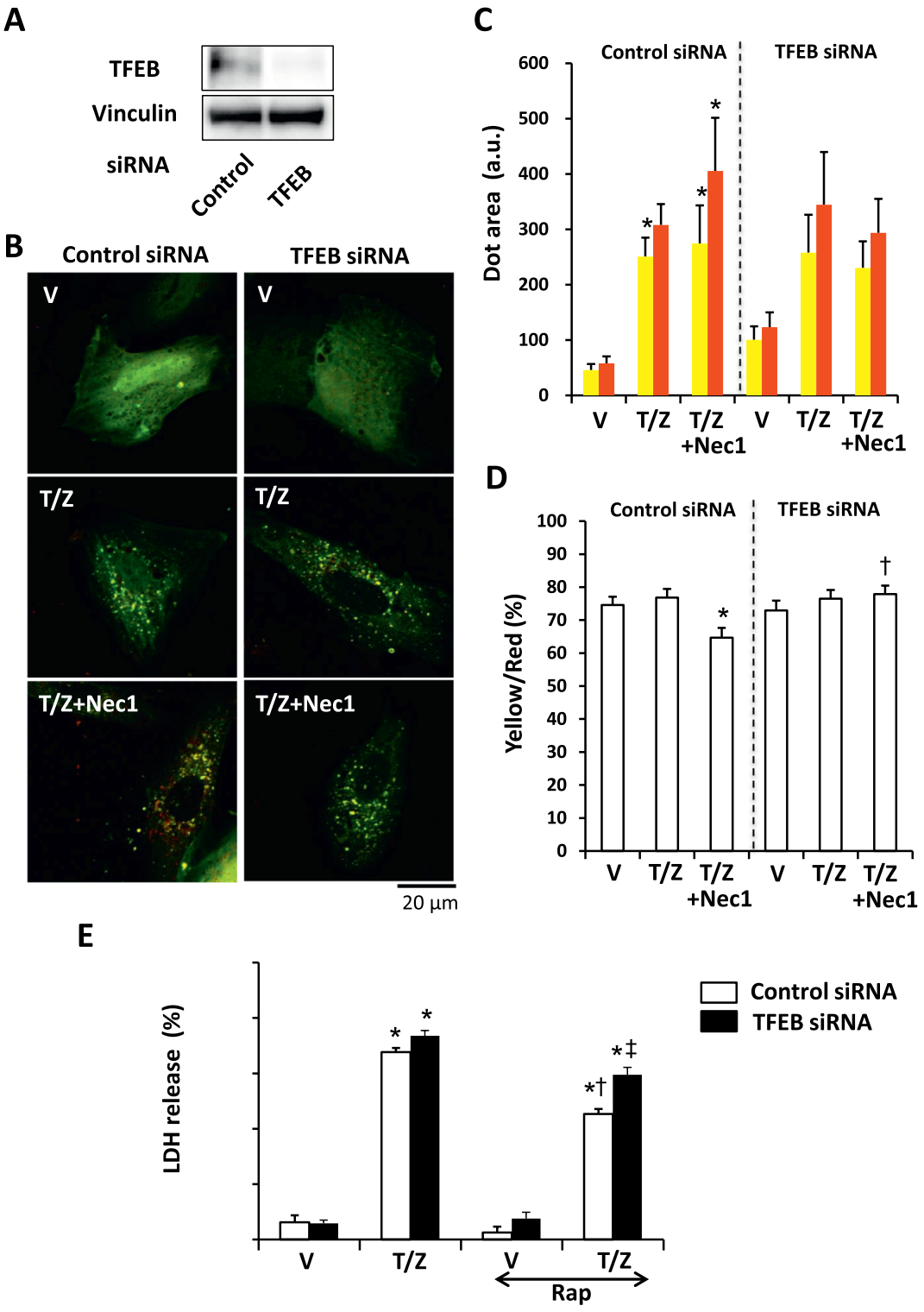

Fig. 8. Effects of TFEB knockdown on restoration of autophagic flux by necrostatin-1 and on suppression of necroptosis by rapamycin in TNF/zVAD-treated cells. (A) Representative blots for TFEB in H9c2 cells with or without knockdown of TFEB. (B) Representative images of H9c2 cells transfected with tandem RFP-GFP-LC3 plasmids at 4 h after pharmacological treatments (magnification 630×). V = vehicle, Nec1 = necrostatin-1, T/Z = TNF-α and zVAD. (C) Group mean data for images captured 4 h after the addition of each drug. Areas of yellow puncta (autophagosomes) and red puncta (autolysosomes) were quantified. N = 35–40 in each group. a.u. = arbitrary units. *$p < 0.05$ vs. V. (D) Group mean data for the ratio of yellow puncta area to red puncta area. *$p < 0.05$ vs. V. $^{\dagger}p < 0.05$ vs. cells transfected with control siRNA and treated with both TNF/zVAD and necrostatin-1. (E) LDH release into the culture medium as a percentage of total cellular LDH activity. Cells were transfected with control siRNA or TFEB siRNA 24 h before treatment with a vehicle (V), TNF/zVAD (T/Z), vehicle + rapamycin (V + Rap), or TNF/zVAD + rapamycin (T/Z + Rap) for 24 h. N = 4 in each group. *$p < 0.05$ vs. vehicle-treated and control siRNA-transfected cells. $^{\dagger}p < 0.05$ vs. T/Z-treated and control siRNA-transfected cells. $^{\ddagger}p < 0.05$ vs. T/Z + Rap-treated and control siRNA-transfected cells.

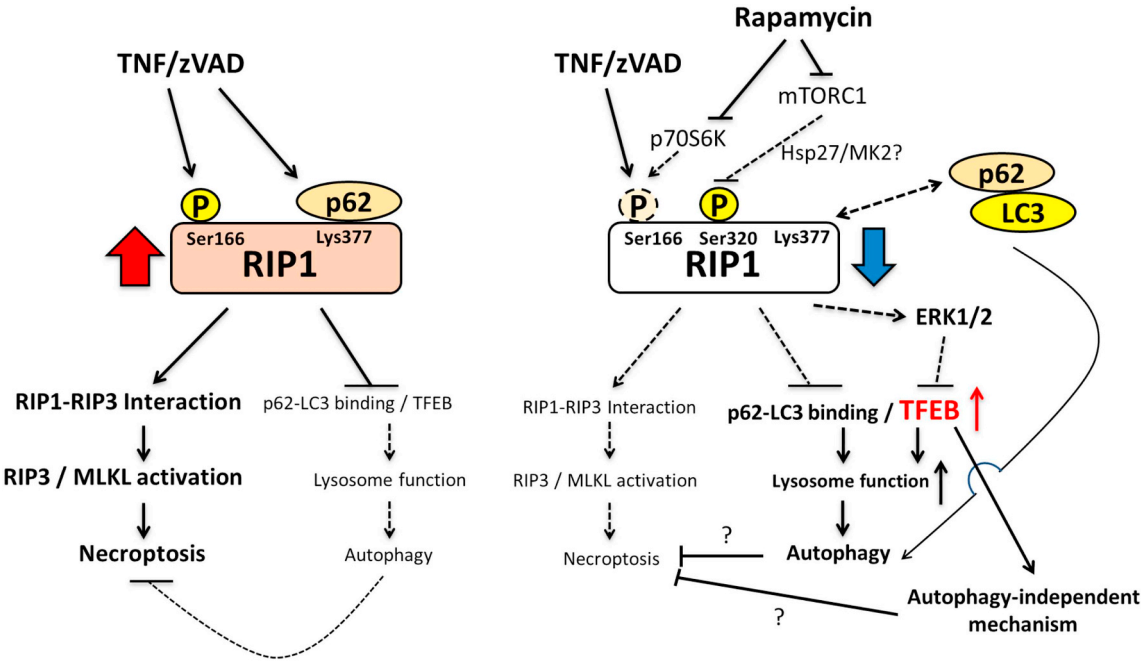

Fig. 9. Proposed mechanism by which mTORC1 inhibition suppresses necroptosis.

cell death was preserved in cells treated with inhibitors of TAK1, IKKα/β, and cIAP (Fig. 2A–C). The findings indicate that the regulators upstream of RIP1 in TNF receptor signaling are not targets for mTORC1 inhibition to protect H9c2 cells from necroptosis. The possibility of contribution of p53 suppression to the protective effect of mTORC1 inhibition was also excluded by the findings that reduction of p53 expression or activity or increase in p53 expression did not change level of necroptosis induced by TNF/zVAD (Supplemental Figs. 17–19).

H9c2 cells have similarities to neonatal cardiomyocytes, including responses to stress, but there are significant differences between H9c2 cells and adult cardiomyocytes. Thus, mechanisms by which mTORC1 inhibition suppresses RIP1 activity and upregulates TFEB function in H9c2 cells might not be extrapolated to adult cardiomyocytes. However, several studies have shown that inhibition of mTORC1 or RIP1 activity upon reperfusion limits myocardial infarct size [7,8,39,40], and we found that administration of rapamycin before reperfusion significantly increased RIP1-Ser320 phosphorylation in rat hearts *in vivo* (Supplemental Fig. 20). The findings support the notion that regulation of RIP1 by mTORC1 is operative and contributes to protection of adult cardiomyocytes.

5. Conclusions

Increase in RIP1-Ser320 in addition to reduction of RIP1-Ser166 phosphorylation plays a major role in mTORC1 inhibition to attenuate RIP1 activation by necroptotic signals in cardiomyocytes. Suppression of RIP1 activity by the dual mechanisms promotes autophagy and prevents necroptotic cell death of cardiomyocytes by a TFEB-mediated mechanism (Fig. 9). The mechanism by which mTORC1 inhibition increases RIP1-Ser320 remains to be further investigated.

Transparency document

The Transparency document associated with this article can be found, in online version.

Acknowledgments

This study was supported by Grant 26461133 (Miura T) and Grant 16K09505 (Yano T) from the Japan Society for the Promotion of Science, Tokyo, Japan; a grant from the Uehara Memorial Foundation, Japan (Miura T); and grants from Takeda Science Foundation, SENSHIN Medical Research Foundation, Suhara Memorial Foundation, the Vehicle Racing Commemorative Foundation, and Novartis Foundation (Yano T).

Declaration of competing interest

The authors report no commercial or proprietary interest in any product or concept discussed in this article.

Appendix A. Supplementary data

Supplementary data to this article can be found online at https://doi.org/10.1016/j.bbadis.2019.165552.

References

[1] T. Vanden Berghe, A. Linkermann, S. Jouan-Lanhouet, H. Walczak, P. Vandenabeele, Regulated necrosis: the expanding network of non-apoptotic cell death pathways, Nat. Rev. Mol. Cell Biol. 15 (2014) 135–147.
[2] A. Linkermann, D.R. Green, Necroptosis, N. Engl. J. Med. 370 (2014) 455–465.
[3] S. Grootjans, T. Vanden Berghe, P. Vandenabeele, Initiation and execution mechanisms of necroptosis: an overview, Cell Death Differ. 24 (2017) 1184–1195.
[4] L. Galluzzi, O. Kepp, F.K. Chan, G. Kroemer, Necroptosis: mechanisms and relevance to disease, Annu. Rev. Pathol. 12 (2017) 103–130.
[5] M. Luedde, M. Lutz, N. Carter, J. Sosna, C. Jacoby, M. Vucur, J. Gautheron, C. Roderburg, N. Borg, F. Reisinger, H.J. Hippe, A. Linkermann, M.J. Wolf, S. Rose-John, R. Lüllmann-Rauch, D. Adam, U. Flögel, M. Heikenwalder, T. Luedde, N. Frey, RIP3, a kinase promoting necroptotic cell death, mediates adverse remodelling after myocardial infarction, Cardiovasc. Res. 103 (2014) 206–216.
[6] T. Zhang, Y. Zhang, M. Cui, L. Jin, Y. Wang, F. Lv, Y. Liu, W. Zheng, H. Shang, J. Zhang, M. Zhang, H. Wu, J. Guo, X. Zhang, X. Hu, C.M. Cao, R.P. Xiao, CaMKII is a RIP3 substrate mediating ischemia- and oxidative stress-induced myocardial necroptosis, Nat. Med. 22 (2016) 175–182.
[7] C.C. Smith, S.M. Davidson, S.Y. Lim, J.C. Simpkin, J.S. Hothersall, D.M. Yellon, Necrostatin: a potentially novel cardioprotective agent? Cardiovasc. Drugs Ther. 21 (2007) 227–233.
[8] M.I. Oerlemans, J. Liu, F. Arslan, K. den Ouden, B.J. van Middelaar, P.A. Doevendans, J.P. Sluijter, Inhibition of RIP1-dependent necrosis prevents adverse cardiac remodeling after myocardial ischemia-reperfusion in vivo, Basic Res. Cardiol. 107 (2012) 270.
[9] A. Szobi, E. Gonçalvesová, Z.V. Varga, P. Leszek, M. Kuśmierczyk, M. Hulman, J. Kyselovič, P. Ferdinandy, A. Adameová, Analysis of necroptotic proteins in failing human hearts, J. Transl. Med. 15 (2017) 86.
[10] L. Li, Y. Chen, J. Doan, J. Murray, J.D. Molkentin, Q. Liu, Transforming growth factor β-activated kinase 1 signaling pathway critically regulates myocardial

survival and remodeling, Circulation 130 (2014) 2162–2172.
[11] N. Vanlangenakker, T. Vanden Berghe, P. Bogaert, B. Laukens, K. Zobel, K. Deshayes, D. Vucic, S. Fulda, P. Vandenabeele, M.J. Bertrand, cIAP1 and TAK1 protect cells from TNF-induced necrosis by preventing RIP1/RIP3-dependent reactive oxygen species production, Cell Death Differ. 18 (2011) 656–665.
[12] J. Geng, Y. Ito, L. Shi, P. Amin, J. Chu, A.T. Ouchida, A.K. Mookhtiar, H. Zhao, D. Xu, B. Shan, A. Najafov, G. Gao, S. Akira, J. Yuan, Regulation of RIPK1 activation by TAK1-mediated phosphorylation dictates apoptosis and necroptosis, Nat. Commun. 8 (2017) 359.
[13] Y.S. Cho, S. Challa, D. Moquin, R. Genga, T.D. Ray, M. Guildford, F.K. Chan, Phosphorylation-driven assembly of the RIP1-RIP3 complex regulates programmed necrosis and virus-induced inflammation, Cell 137 (2009) 1112–1123.
[14] D.W. Zhang, J. Shao, J. Lin, N. Zhang, B.J. Lu, S.C. Lin, M.Q. Dong, J. Han, RIP3, an energy metabolism regulator that switches TNF-induced cell death from apoptosis to necrosis, Science 325 (2009) 332–336.
[15] L. Sun, H. Wang, Z. Wang, S. He, S. Chen, D. Liao, L. Wang, J. Yan, W. Liu, X. Lei, X. Wang, Mixed lineage kinase domain-like protein mediates necrosis signaling downstream of RIP3 kinase, Cell 148 (2012) 213–227.
[16] Z. Cai, S. Jitkaew, J. Zhao, H.C. Chiang, S. Choksi, J. Liu, Y. Ward, L.G. Wu, Z.G. Liu, Plasma membrane translocation of trimerized MLKL protein is required for TNF-induced necroptosis, Nat. Cell Biol. 16 (2014) 55–65.
[17] L. Galluzzi, O. Kepp, G. Kroemer, MLKL regulates necrotic plasma membrane permeabilization, Cell Res. 24 (2014) 139–140.
[18] N. Mizushima, Y. Ohsumi, T. Yoshimori, Autophagosome formation in mammalian cells, Cell Struct. Funct. 27 (2002) 421–429.
[19] A. Nakai, O. Yamaguchi, T. Takeda, Y. Higuchi, S. Hikoso, M. Taniike, S. Omiya, I. Mizote, Y. Matsumura, M. Asahi, K. Nishida, M. Hori, N. Mizushima, K. Otsu, The role of autophagy in cardiomyocytes in the basal state and in response to hemodynamic stress, Nat. Med. 13 (2007) 619–624.
[20] H. Kanamori, G. Takemura, K. Goto, R. Maruyama, K. Ono, K. Nagao, A. Tsujimoto, A. Ogino, T. Takeyama, T. Kawaguchi, T. Watanabe, M. Kawasaki, T. Fujiwara, H. Fujiwara, M. Seishima, S. Minatoguchi, Autophagy limits acute myocardial infarction induced by permanent coronary artery occlusion, Am. J. Physiol. Heart Circ. Physiol. 300 (2011) H2261–H2271.
[21] H. Murase, A. Kuno, T. Miki, M. Tanno, T. Yano, H. Kouzu, S. Ishikawa, T. Tobisawa, M. Ogasawara, K. Nishizawa, T. Miura, Inhibition of DPP-4 reduces acute mortality after myocardial infarction with restoration of autophagic response in type 2 diabetic rats, Cardiovasc. Diabetol. 14 (2015) 103.
[22] Y.C. Ye, L. Yu, H.J. Wang, S. Tashiro, S. Onodera, T. Ikejima, TNFα-induced necroptosis and autophagy via supression of the p38-NF-κB survival pathway in L929 cells, J. Pharmacol. Sci. 117 (2011) 160–169.
[23] P. Kharaziha, D. Chioureas, G. Baltatzis, P. Fonseca, P. Rodriguez, V. Gogvadze, L. Lennartsson, A.C. Björklund, B. Zhivotovsky, D. Grandér, L. Egevad, S. Nilsson, T. Panaretakis, Sorafenib-induced defective autophagy promotes cell death by necroptosis, Oncotarget 6 (2015) 37066–37082.
[24] M.L. Goodall, B.E. Fitzwalter, S. Zahedi, M. Wu, D. Rodriguez, J.M. Mulcahy-Levy, D.R. Green, M. Morgan, S.D. Cramer, A. Thorburn, The autophagy machinery controls cell death switching between apoptosis and necroptosis, Dev. Cell 37 (2016) 337–349.
[25] M.M. Young, Y. Takahashi, O. Khan, S. Park, T. Hori, J. Yun, A.K. Sharma, S. Amin, C.D. Hu, J. Zhang, M. Kester, H.G. Wang, Autophagosomal membrane serves as platform for intracellular death-inducing signaling complex (iDISC)-mediated caspase-8 activation and apoptosis, J. Biol. Chem. 287 (2012) 12455–12468.
[26] M. Ogasawara, T. Yano, M. Tanno, K. Abe, S. Ishikawa, T. Miki, A. Kuno, T. Tobisawa, S. Muratsubaki, K. Ohno, Y. Tatekoshi, K. Nakata, W. Ohwada, T. Miura, Suppression of autophagic flux contributes to cardiomyocyte death by activation of necroptotic pathways, J. Mol. Cell. Cardiol. 108 (2017) 203–213.
[27] T. Yonekawa, G. Gamez, J. Kim, A.C. Tan, J. Thorburn, J. Gump, A. Thorburn, M.J. Morgan, RIP1 negatively regulates basal autophagic flux through TFEB to control sensitivity to apoptosis, EMBO Rep. 16 (2015) 700–708.
[28] S. Kimura, T. Noda, T. Yoshimori, Dissection of the autophagosome maturation process by a novel reporter protein, tandem fluorescent-tagged LC3, Autophagy 3 (2007) 452–460.
[29] K. Nishizawa, T. Yano, M. Tanno, T. Miki, A. Kuno, T. Tobisawa, M. Ogasawara, S. Muratsubaki, K. Ohno, S. Ishikawa, T. Miura, Chronic treatment with an erythropoietin receptor ligand prevents chronic kidney disease-induced enlargement of myocardial infarct size, Hypertension 68 (2016) 697–706.
[30] D.E. Christofferson, Y. Li, J. Hitomi, W. Zhou, C. Upperman, H. Zhu, S.A. Gerber, S. Gygi, J. Yuan, A novel role for RIP1 kinase in mediating TNFα production, Cell Death Dis. 3 (2012) e320.
[31] A. Degterev, J. Hitomi, M. Germscheid, I.L. Ch'en, O. Korkina, X. Teng, D. Abbott, G.D. Cuny, C. Yuan, G. Wagner, S.M. Hedrick, S.A. Gerber, A. Lugovskoy, J. Yuan, Identification of RIP1 kinase as a specific cellular target of necrostatins, Nat. Chem. Biol. 4 (2008) 313–321.
[32] S.B. Berger, V. Kasparcova, S. Hoffman, B. Swift, L. Dare, M. Schaeffer, C. Capriotti, M. Cook, J. Finger, A. Hughes-Earle, P.A. Harris, W.J. Kaiser, E.S. Mocarski, J. Bertin, P.J. Gough, RIP1 kinase activity is dispensable for normal development but is a key regulator of inflammation in SHARPIN-deficient mice, J. Immunol. 192 (2014) 5476–5480.
[33] Y. Dondelinger, S. Jouan-Lanhouet, T. Divert, E. Theatre, J. Bertin, P.J. Gough, P. Giansanti, A.J. Heck, E. Dejardin, P. Vandenabeele, M.J. Bertrand, NF-κB-independent role of IKKα/IKKβ in preventing RIPK1 kinase-dependent apoptotic and necroptotic cell death during TNF signaling, Mol. Cell 60 (2015) 63–76.
[34] Y. Dondelinger, P. Vandenabeele, M.J. Bertrand, Regulation of RIPK1's cell death function by phosphorylation, Cell Cycle 15 (2016) 5–6.
[35] Y. Dondelinger, T. Delanghe, D. Rojas-Rivera, D. Priem, T. Delvaeye, I. Bruggeman, F. Van Herreweghe, P. Vandenabeele, M.J. Bertrand, MK2 phosphorylation of RIPK1 regulates TNF-mediated cell death, Nat. Cell Biol. 19 (2017) 1237–1247.
[36] M.B. Menon, J. Gropengießer, J. Fischer, L. Novikova, A. Deuretzbacher, J. Lafera, H. Schimmeck, N. Czymmeck, N. Ronkina, A. Kotlyarov, M. Aepfelbacher, M. Gaestel, K. Ruckdeschel, $p38^{MAPK}$/MK2-dependent phosphorylation controls cytotoxic RIPK1 signalling in inflammation and infection, Nat. Cell Biol. 19 (2017) 1248–1259.
[37] I. Jaco, A. Annibaldi, N. Lalaoui, R. Wilson, T. Tenev, L. Laurien, C. Kim, K. Jamal, S. Wicky John, G. Liccardi, D. Chau, J.M. Murphy, G. Brumatti, R. Feltham, M. Pasparakis, J. Silke, P. Meier, MK2 phosphorylates RIPK1 to prevent TNF-induced cell death, Mol. Cell 66 (2017) (698-710.e5).
[38] T. Yano, M. Ferlito, A. Aponte, A. Kuno, T. Miura, E. Murphy, C. Steenbergen, Pivotal role of mTORC2 and involvement of ribosomal protein S6 in cardioprotective signaling, Circ. Res. 114 (2014) 1268–1280.
[39] H.H. Chen, C. Mekkaoui, H. Cho, S. Ngoy, B. Marinelli, P. Waterman, M. Nahrendorf, R. Liao, L. Josephson, D.E. Sosnovik, Fluorescence tomography of rapamycin-induced autophagy and cardioprotection in vivo, Circ. Cardiovasc. Imaging 6 (2013) 441–447.
[40] S.M. Filippone, A. Samidurai, S.K. Roh, C.K. Cain, J. He, F.N. Salloum, R.C. Kukreja, A. Das, Reperfusion therapy with rapamycin attenuates myocardial infarction through activation of AKT and ERK, Oxidative Med. Cell. Longev. 2017 (2017) 4619720.
[41] D. Ofengeim, J. Yuan, Regulation of RIP1 kinase signalling at the crossroads of inflammation and cell death, Nat. Rev. Mol. Cell Biol. 14 (2013) 727–736.
[42] N. Herranz, S. Gallage, M. Mellone, T. Wuestefeld, S. Klotz, C.J. Hanley, S. Raguz, J.C. Acosta, A.J. Innes, A. Banito, A. Georgilis, A. Montoya, K. Wolter, G. Dharmalingam, P. Faull, T. Carroll, J.P. Martínez-Barbera, P. Cutillas, F. Reisinger, M. Heikenwalder, R.A. Miller, D. Withers, L. Zender, G.J. Thomas, J. Gil, mTOR regulates MAPKAPK2 translation to control the senescence-associated secretory phenotype, Nat. Cell Biol. 17 (2015) 1205–1217.
[43] R. Wu, H. Kausar, P. Johnson, D.E. Montoya-Durango, M. Merchant, M.J. Rane, Hsp27 regulates Akt activation and polymorphonuclear leukocyte apoptosis by scaffolding MK2 to Akt signal complex, J. Biol. Chem. 282 (2007) 21598–21608.
[44] W. Cai, J.L. Rudolph, S.M. Harrison, L. Jin, A.L. Frantz, D.A. Harrison, et al., An evolutionarily conserved Rit GTPase-p38 MAPK signaling pathway mediates oxidative stress resistance, Mol. Biol. Cell 22 (2011) 3231–3241.
[45] T. Noda, Regulation of autophagy through TORC1 and mTORC1, Biomolecules 7 (2017) E52.
[46] Y. Rabanal-Ruiz, E.G. Otten, V.I. Korolchuk, mTORC1 as the main gateway to autophagy, Essays Biochem. 61 (2017) 565–584.
[47] J. Kim, M. Kundu, B. Viollet, K.L. Guan, AMPK and mTOR regulate autophagy through direct phosphorylation of Ulk1, Nat. Cell Biol. 13 (2011) 132–141.
[48] B. Pan, H. Zhang, T. Cui, X. Wang, TFEB activation protects against cardiac proteotoxicity via increasing autophagic flux, J. Mol. Cell. Cardiol. 113 (2017) 51–62.
[49] C. Settembre, C. Di Malta, V.A. Polito, M. Garcia Arencibia, F. Vetrini, S. Erdin, S.U. Erdin, T. Huynh, D. Medina, P. Colella, M. Sardiello, D.C. Rubinsztein, A. Ballabio, TFEB links autophagy to lysosomal biogenesis, Science 332 (2011) 1429–1433.
[50] A. Roczniak-Ferguson, C.S. Petit, F. Froehlich, S. Qian, J. Ky, B. Angarola, T.C. Walther, S.M. Ferguson, The transcription factor TFEB links mTORC1 signaling to transcriptional control of lysosome homeostasis, Sci. Signal. 5 (2012) ra42.
[51] S. Inokuchi-Shimizu, E.J. Park, Y.S. Roh, L. Yang, B. Zhang, J. Song, S. Liang, M. Pimienta, K. Taniguchi, X. Wu, K. Asahina, W. Lagakos, M.R. Mackey, S. Akira, M.H. Ellisman, D.D. Sears, J.M. Olefsky, M. Karin, D.A. Brenner, E. Seki, TAK1-mediated autophagy and fatty acid oxidation prevent hepatosteatosis and tumorigenesis, J. Clin. Invest. 124 (2014) 3566–3578.
[52] J.H. Shin, S.H. Min, S.J. Kim, Y.I. Kim, J. Park, H.K. Lee, O.J. Yoo, TAK1 regulates autophagic cell death by suppressing the phosphorylation of p70 S6 kinase 1, Sci. Rep. 3 (2013) 1561.
[53] A. Criollo, L. Senovilla, H. Authier, M.C. Maiuri, E. Morselli, I. Vitale, O. Kepp, E. Tasdemir, L. Galluzzi, S. Shen, M. Tailler, N. Delahaye, A. Tesniere, D. De Stefano, A.B. Younes, F. Harper, G. Pierron, S. Lavandero, L. Zitvogel, A. Israel, V. Baud, G. Kroemer, The IKK complex contributes to the induction of autophagy, EMBO J. 29 (2010) 619–631.
[54] O.A. Brady, J.A. Martina, R. Puertollano, Emerging roles for TFEB in the immune response and inflammation, Autophagy 14 (2018) 181–189.
[55] D.L. Medina, A. Fraldi, V. Bouche, F. Annunziata, G. Mansueto, C. Spampanato, C. Puri, A. Pignata, J.A. Martina, M. Sardiello, M. Palmieri, R. Polishchuk, R. Puertollano, A. Ballabio, Transcriptional activation of lysosomal exocytosis promotes cellular clearance, Dev. Cell 21 (2011) 421–430.